

Experiments on Form Factors *

Tord Johansson¹⁾¹ Department of Physics and Astronomy, Uppsala University, Uppsala, Sweden

Abstract: The experimental situation for ground state baryon electromagnetic form factors in the space-like and the time-like regions is reviewed together with an outlook.

Key words: baryon, proton, neutron, hyperon, electromagnetic form factor

PACS: 13.40.Gp, 14.20.Dh, 14.20.Jn

1 Introduction

Electromagnetic Form Factors (EMFF's) are among the most basic properties that describe the internal structure of hadrons. They give direct access to their spatial charge and magnetisation distributions. The knowledge of these is, however, far from complete and several open questions are awaiting their answer. This review deals with EMFF's of ground state baryons. These are studied in two kinematically different domains: The space-like (SL) region is studied by elastic electron-baryon scattering, whereas the time-like (TL) region is studied in electron-positron annihilation into a baryon-antibaryon pair, or vice versa. The topic of elastic EMFF's has been addressed recently by several review articles and the reader is referred to these (Refs. [1–4]) for a more thorough presentation.

2 Space-like form factors

The most abundant information on EMFF's comes from elastic scattering of electrons on nucleons. This process is visualised in Fig. 1.

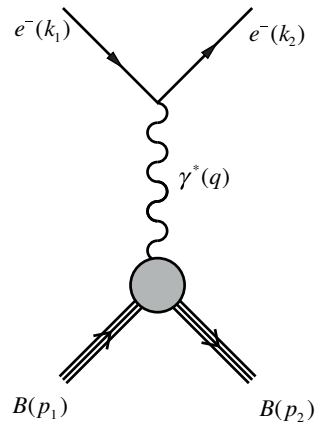


Fig. 1. Feynman diagram of the Born term for elastic electron baryon scattering.

It has been assumed that this single virtual photon exchange process gives a good description of the scattering reaction. The upper electromagnetic vertex in Fig. 1 is well known and the baryon electromagnetic properties are contained in the lower non-pointlike baryon vertex. The 4-momentum squared, q^2 , is a negative quantity in the SL region and one therefore usually defines $Q^2 = -q^2$. The baryon vertex matrix element can then be written as

$$\Gamma^\mu = F_1^B(Q^2)\gamma^\mu + \frac{\kappa}{2M_B}F_2^B(Q^2)i\sigma^{\mu\nu}q_\nu. \quad (1)$$

where $F_1^B(Q^2)$ and $F_2^B(Q^2)$ are related to the non-helicity-flip and helicity flip part of the hadronic current and are named Dirac and Pauli EMFF's, respectively. It is convenient to re-write these EMFF's in terms of the Sachs FF's:

Received 30 Nov. 2015

* Supported by The Swedish Research Council

1) E-mail: tord.johansson@physics.uu.se

$$\begin{aligned}
 G_E &= F_1 - \tau F_2; \tau = \frac{Q^2}{4M_B^2}. \\
 G_M &= F_1 + F_2.
 \end{aligned}
 \quad (2)$$

The Sachs FF's correspond, non-relativistically, to the Fourier transformations of the transverse charge and magnetic spatial distributions in the Breit frame. However, the interpretation becomes more complicated as the energy increases (see *e.g.* Ref. [1]).

The space-like elastic EMFF's have traditionally been obtained in terms of G_E^2 and G_M^2 via the Rosenbluth separation technique as

$$\begin{aligned}
 \frac{d\sigma}{d\Omega} &= \left(\frac{d\sigma}{d\Omega} \right)_{Mott} \frac{E_e}{E_{beam}} \frac{1}{1+\tau} \left(G_E^2 + \frac{\tau}{\epsilon} G_M^2 \right). \\
 \epsilon &= \frac{1}{1+2(1+\tau)\tan^2\theta_e/2}.
 \end{aligned}
 \quad (3)$$

where E_{beam} and E_e are the energy of the incoming and scattered electron, respectively, θ_e the electron scattering angle, and ϵ is the virtual photon polarisation[1]. The linear dependence on τ and ϵ of Eq. (3) allows for a definition of a reduced cross section as

$$\sigma_{red} = \frac{\epsilon(1+\tau)}{\tau} \frac{E_{beam}}{E_e} \frac{d\sigma}{d\Omega} / \left(\frac{d\sigma}{d\Omega} \right)_{Mott} = G_M^2 + \frac{\epsilon}{\tau} G_E^2. \quad (4)$$

Hence, σ_{red} has a linear dependence on ϵ at a given Q^2 with a slope proportional to G_E^2 and an intercept at G_M^2 . G_E^2 and G_M^2 are therefore extracted from fits to experimental data by measuring the cross section at a given Q^2 at different energies (ϵ). It should be noted that the $1/\tau$ factor makes it difficult to determine G_E^2 at higher Q^2 by this method. In turn, corrections to the one-photon approximation can give sizeable impact on the small quantity G_E^2/τ and therefore on the extraction of G_E .

2.1 Proton space-like FF's

Many data have been collected on elastic electron scattering on the proton since the pioneering experiments by Hofstadter [5] in the 50's. In the static limit $G_{Mp} = \mu_p G_{Ep}$ and this is roughly consistent with data. Furthermore, the Q^2 dependence of the proton EMFF's is well characterised by a dipole behaviour: $G_D = (1 + Q^2/.71GeV^2)^2$. This is depicted in Fig. 2 where the G_E and G_M/μ_p are divided by G_D .

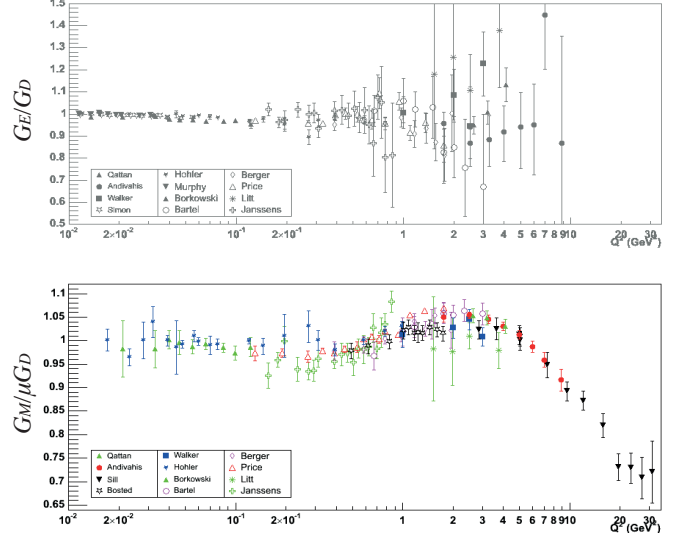


Fig. 2. Experimental data on the proton G_E (upper figure) and G_M/μ_p (lower figure) divided by the dipole function G_D (see Refs. [1, 3] and references therein).

A rather coherent picture has emerged from these data. More recently, however, polarisation measurements have brought a new dimension to this topic. Two techniques have evolved:

- Polarisation transfer experiments. Here a longitudinally polarised electron transfers its polarisation to the recoiling proton. The transverse (P_t) and longitudinal (P_l) polarisation of the proton is subsequently measured via a secondary scattering. The G_E/G_M ratio is then determined from

$$\frac{G_E}{G_M} = -\frac{P_t}{P_l} \frac{(E_{beam} + E_e)}{2M_p} \tan \frac{\theta_e}{2}. \quad (5)$$

- Polarised proton target experiments. Here one measures the asymmetry between the cross sections for the two electron helicity states, $A = (\sigma_+ - \sigma_-)/(\sigma_+ + \sigma_-)$.

Both these methods have the advantage that they do not have the $1/\tau$ suppression of the G_E term and that many systematical effects cancel when taking ratios. See *e.g.* Ref. [1] for more details. It came as a big surprise when the polarisation measurements of $\mu_p G_{Ep}/G_{Mp}$ from JLab showed a distinct difference from the results obtained from the Rosenbluth separation method as shown in Fig. 3.

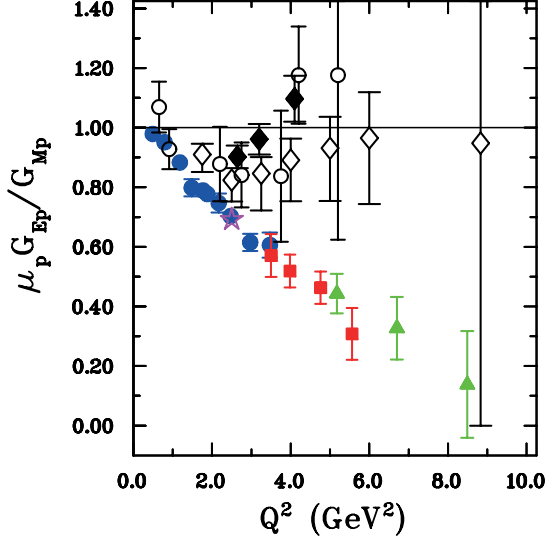


Fig. 3. Experimental data on the ratio $\mu_p G_{E_p}/G_{M_p}$ extracted using Rosenbluth separation (black symbols) and polarisation measurements (coloured symbols). Adapted from Ref. [3]

Whereas the Rosenbluth separation indicates a constant ratio up to a Q^2 of 10 GeV^2 the polarisation data show a linear decrease of the ratio with Q^2 , even indicating a zero-crossing in the region of $Q^2 \approx 10 \text{ GeV}^2$. Why this difference? It is generally believed that the polarisation data are more accurate and one plausible explanation is that the Rosenbluth separation is much more sensitive to contributions from two-photon exchanges. This would then be reflected by this difference. A way to test this hypothesis is to measure the ratio $R = \sigma(e^+p)/\sigma(e^-p)$ since the two-photon contribution enters with different signs for the two cases. It is not straightforward, however, to make precise comparisons of different experiments due to different systematical uncertainties. A way out of this difficulty is offered by the CLAS experiment at JLab by using a beam that simultaneously contains electrons and positrons created by pair-production of high energy photons [6]. The result is not conclusive due to the statistics but points towards the two-photon hypothesis being correct. Another proton puzzle is the difference in the charge RMS radius extracted from electron scattering data at low Q^2 and Lamb-shift measurements in muonic and ordinary hydrogen. This topic is covered in several contributions to these proceedings and the reader is referred to these contributions for more details.

2.2 Neutron space-like FF's

Much less data are available on neutron space-like FF's. G_{E_n} and G_{M_n} have traditionally been extracted from quasi-elastic electron scattering from deuteron targets. The Rosenbluth separation requires large correc-

tions in this case, however. More recent polarisation measurements employ polarised deuteron and ^3He targets.

The data on G_{M_n} agree well with the same dipole expression as for the proton, as can be seen in Fig. 4 pointing to the similarity between G_{M_n} and G_{M_p} . See *e.g.* Refs. [1, 2] for more details.

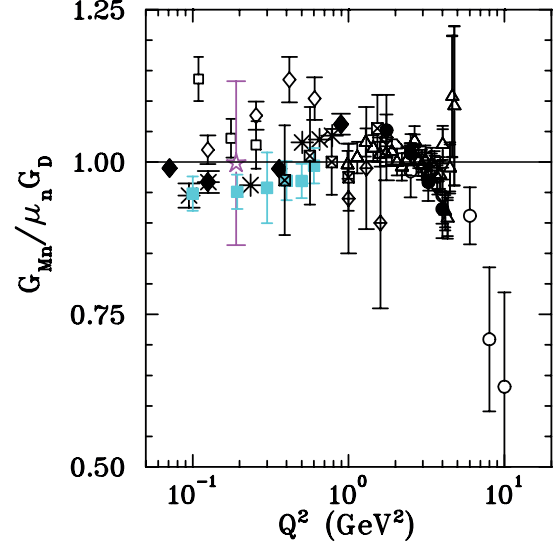


Fig. 4. Experimental data on the ratio $G_{M_n}/\mu_n G_D$ extracted using Rosenbluth separation (black symbols) and polarisation measurements (coloured symbols). Adapted from Ref. [3].

3 Time-like form factors

Baryon form factors in the time-like region are extracted from measurements of the produced particles in $e^-e^+ \leftrightarrow B\bar{B}$ reactions as depicted in Fig. 5.

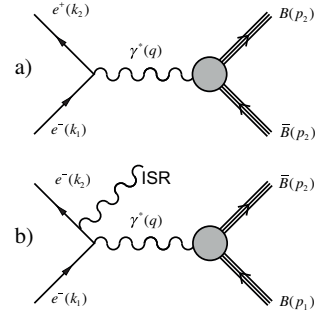


Fig. 5. Feynman diagrams of the Born term for processes used to determine baryon time-like FF's: a) Direct annihilation and, b) Initial state radiation.

The FF's in the TL region are complex functions

$$\begin{aligned} \text{Re}[G_E(q^2)G_M^*(q^2)] &= |G_E(q^2)||G_M(q^2)| \cos \phi \\ \text{Im}[G_E(q^2)G_M^*(q^2)] &= |G_E(q^2)||G_M(q^2)| \sin \phi \end{aligned} \quad (6)$$

where ϕ is the relative phase between G_E and G_M . This relative phase gives polarisation effects on the final state even if the initial state is unpolarised. Assuming one photon exchange (Born term) one can extract information on the TL FF's from the differential cross section according to

$$\frac{d\sigma}{d\cos\theta} = \frac{\alpha^2\beta C}{4q^2} (|G_M|^2(1+\cos^2\theta) + \frac{1}{\tau}|G_E|^2\sin^2\theta).$$

$$\tau = \frac{q^2}{4M_B^2}, \beta = \sqrt{1-1/\tau}, C = y/(1-e^{-y}), y = \pi\alpha/\beta \quad (7)$$

where C is a Coulomb factor. At the kinematical threshold are $\tau=1$ and $G_E = G_M$. It should be noted that the Coulomb factor implies a non-zero cross section at threshold for charged final states, whereas $C = 1$ for the neutral case. $Re[G_E(q^2)G_M^*(q^2)]$ and $Im[G_E(q^2)G_M^*(q^2)]$ are related to the polarisation P_y and the spin correlation C_{xz} by the relations [7]

$$P_y = -\frac{\sin 2\theta \text{Im}[G_E G_M^*]/\sqrt{\tau}}{(|G_E|^2 \sin^2\theta)/\tau + |G_M|^2(1+\cos^2\theta)} = -\frac{\sin 2\theta \sin\phi/\tau}{R \sin^2\theta/\sqrt{\tau} + (1+\cos^2\theta)} \quad (8)$$

and

$$C_{xz} = -\frac{\sin 2\theta \text{Re}[G_E G_M^*]/\sqrt{\tau}}{(|G_E|^2 \sin^2\theta)/\tau + |G_M|^2(1+\cos^2\theta)} = -\frac{\sin 2\theta \cos\phi/\tau}{R \sin^2\theta/\tau + (1+\cos^2\theta)/R}. \quad (9)$$

The coordinate system is defined such that y is normal to the scattering plane, z in the direction of the outgoing (anti)baryon and x defines a right handed system.

The TL FF q^2 dependence is either obtained from an energy scan as shown in Fig. 5 a) or by using the initial state radiation (ISR) technique as shown in Fig 5b). The latter allows for an energy scan while staying at a fixed energy due to the energy distributions of the ISR photons. This has the advantage that all q^2 are sampled simultaneously, and by this minimising systematic uncertainties. Another advantage is that the final state baryons are not produced at rest at the kinematical threshold using ISR. All this is, however, at the expense of a lower luminosity.

The data from experiments in the TL region is often limited and do not allow for a statistically significant determination of $|G_E|^2$ and $|G_M|^2$ individually. Most experiments quote therefore an effective FF, $|G_{eff}|^2$, based on the total cross section

$$|G_{eff}| = \left(\frac{\sigma_{tot}}{\frac{4\pi\alpha^2\beta}{3q^2} C \left(1 + \frac{2M_B^2}{q^2}\right)} \right)^{\frac{1}{2}} = \left(\frac{q^2 |G_M|^2 + 2M_B^2 |G_E|^2}{q^2 + 2M_B^2} \right)^{\frac{1}{2}}. \quad (10)$$

3.1 Proton time-like FF's

A compilation of proton effective time-like FF is shown in Fig. 6. The most extensive data sets come from the BaBar experiment (Refs. [8, 9]) using ISR whereas the other data points are taken at fixed energies (see Ref [10] and references therein).

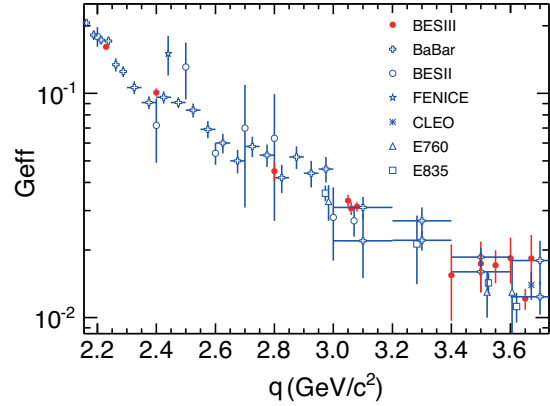


Fig. 6. Plot of the proton effective time-like form factor from Ref. [10].

There are several open questions concerning proton TL FF's. There is an unexpected increase of $|G_{eff}|$, *i.e.* an increase of the cross section with respect to phase space behaviour as one approaches the kinematical threshold in e^+e^- collisions. There are also discrepancies between the experiments that have extracted $|G_E|/|G_M|$ near threshold [8, 11]. There are recent results from BESIII that in this region but the statistics are not sufficient to be decisive [10]. Furthermore, there is a structure in the BaBar data in the region of $q^2 < 3$ GeV/c as can be seen in Fig 6. The reason for this structure is not known but it has recently been pointed out in Ref. [12] that the data seem to exhibit an oscillatory pattern, hinting towards some kind of interference effect.

3.2 Neutron time-like FF's

Data are very scarce on the neutron time-like FF's. Few data points on the effective form factor exist from the FENICE experiment at DAΦNE [13] and, more recently, from the SND experiment at VEPP-2000 [14]. These data are compatible with the corresponding data on the proton. More details on this topic are given in the contribution from A. Korol in these proceedings.

3.3 Hyperon time-like FF's

Only time-like FF's are accessible for the hyperons due to their short lifetime. Their production in e^+e^- collision is therefore the best way to study their electromagnetic structure. Hyperons also offer a straightforward access to polarisation variables since many of them decay via parity violating weak decays.

Data exist from BaBar [15], CLEO-C [16]. New, preliminary data from BESIII are presented at this workshop by Y. Wang. The BaBar experiment did employ the ISR technique whereas CLEO-C and BESIII use discrete energies. The most complete data set comes from the BaBar experiment which encompasses data on the effective FF of both Λ and Σ^0 [15]. These data are displayed in Fig. 7.

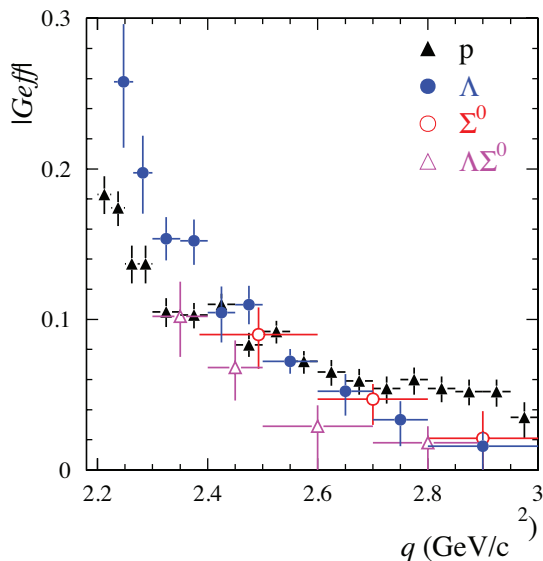


Fig. 7. Plot of hyperon effective TL FF from the BaBar experiment. The proton effective TL FF is also displayed for comparison. Adapted from Ref. [15].

One remarkable feature about these data is that there seems to be an enhancement of the cross section as one approaches the kinematical threshold. This is further emphasised in new preliminary data from BESIII presented at this meeting. None of the published data on the hyperon channels have large enough statistics to determine $|G_E|$ and $|G_M|$ or even their ratio with any statistical accuracy. This situation is about to be changed by a recent measurement by BESIII as reported by Y. Wang. There is even the prospect to measure the phase, including the sign, between $|G_E|$ and $|G_M|$ for the Λ hyperons.

4 Conclusions and outlook

A lot of progress has been made over the last years on baryon ground state form factors but we still lack a unified understanding of their space-like and time-like form

factors. These data have also raised new questions that need to be answered.

- Up to which momentum transfers is the Rosenbluth separation technique valid and how sensitive are different experimental observables?
- Is the proton radius puzzle real?
- What is the reason for the structure in the proton time-like FF?
- What is the reason for the threshold enhancement for baryon time-like FF's?
- From what momentum transfer do interpretations based on perturbative QCD for space-like and time-like FF's start to become valid?

New data from JLab 12 GeV, BESIII and the PANDA experiment at FAIR will hopefully be decisive in answering these questions.

References

- 1 Perdrisat C.F., Punjabi V. and Vanderhaegen M. Nucleon electromagnetic form factors. *Prog. Part. Nucl. Phys.* 59, 2007, 694.
- 2 Denig A. and Salmé V. Nucleon electromagnetic form factors in the timelike region. *Prog. Part. Nucl. Phys.* 68, 2013, 113.
- 3 Punjabi V. *et al.* The Structure of the Nucleon: Elastic Electromagnetic Form Factors. *Eur. Phys. J A* 51, 2015, 79, arXiv:1503.01452v4 [nucl-ex].
- 4 Pacetti S., Baldini Ferrolli R. and Tomasi-Gustafsson E. Proton electromagnetic form factors: Basic notions, present achievements and future perspectives, *Phys. Rep.* 550-551, 2015, 1.
- 5 Hofstadter R. and McAllister R.W. Electron Scattering from the Proton, *Phys. Rev.* 98, 1955, 217.
- 6 Adikaram D. *et al.* Towards a Resolution of the Proton Form Factor Problem: New Electron and Positron Scattering Data, *Phys. Rev. Lett.* 114, 2015, 062003.
- 7 Dubničkova A.Z., Dubnička S. and Rekaló M.P., Investigation of the baryon electromagnetic structure by polarization effects in $e^+e^- \rightarrow B\bar{B}$ processes, *Nuov. Cim A* 109, 1996, 241.
- 8 Lees J.P. *et al.* Study of $e^+e^- \rightarrow p\bar{p}$ via initial state radiation at BaBar, *Phys.Rev. D* 87, 2013, 092005.
- 9 Lees J.P. *et al.* Measurement of the $e^+e^- \rightarrow p\bar{p}$ cross section in the energy range from 3.0 to 6.5 GeV/c, *Phys.Rev. D* 88, 2013, 072009.
- 10 Ablikim M. *et al.* Measurement of the proton form factor by studying $e^+e^- \rightarrow p\bar{p}$, *Phys. Rev. D* 91, 2015, 112004.
- 11 Bardin G. *et al.* Determination of the electric and magnetic form factors of the proton in the time-like region, *Nucl. Phys. B* 411, 1994, 3.
- 12 Bianconi A. and Tomasi-Gustafsson E. Periodic Interference Structures in the Timelike Proton Form Factor, *Phys. Rev. Lett.* 114, 2015, 232301.
- 13 Antonelli A. *et al.* The first measurement of the neutron electromagnetic form factors in the time-like region, *Nucl. Phys. B* 517, 1998, 3.
- 14 Achasov M.N. *et al.* Study of the process $e^+e^- \rightarrow n\bar{n}$ at the VEPP-2000 e^+e^- collider with the SND detector, *Phys. Rev. D* 90, 2014, 112007.
- 15 Aubert B. *et al.* Study of $e^+e^- \rightarrow \Lambda\bar{\Lambda}, \Lambda\bar{\Sigma}^0, \Sigma^0\bar{\Sigma}^0$ using initial state radiation with BABAR, *Phys. Rev. D* 76, 2007, 092006.
- 16 Dobbs S. *et al.* First measurements of timelike form factors of the hyperons $\Lambda^0, \Sigma^0, \Sigma^+, \Xi^0, \Xi^-$, and Ω^- , and evidence of diquark correlations., *Phys. Lett. B* 739, 2014, 90.